This is a postprint of an article published by Elsevier . The final version of Seif Eddine Fenni, Jun Wang, Nacerddine Haddaoui, Basil D. Favis, Alejandro J. Müller, Dario Cavallo, **Crystallization and self-nucleation of PLA, PBS and PCL in their immiscible binary and ternary blends**, *Thermochimica Acta*, (2019), 677, 117-130,is available at https://doi.org/10.1016/j.tca.2019.03.015
© 2019 This manuscript version is made available under the CC-BY-NC-ND 4.0 license http://creativecommons.org/licenses/by-nc-nd/4.0/

Crystallization and self-nucleation of PLA, PBS and PCL in their immiscible binary and ternary blends

Seif Eddine Fenni [1,2], Jun Wang [3], Nacerddine Haddaoui [1], Basil D. Favis [3], Alejandro J. Müller [4,5,*], and Dario Cavallo [2,*]

[1] Laboratory of Physical-Chemistry of High Polymers (LPCHP), Faculty of Technology, University of Ferhat ABBAS Sétif-1, 19000 Sétif, Algeria

[2] Department of Chemistry and Industrial Chemistry, University of Genova, via Dodecaneso, 31 - 16146 Genova, Italy

[3] CREPEC, Department of Chemical Engineering, École Polytechnique de Montréal, Montréal, Québec H3C3A7, Canada.

[4] POLYMAT and Polymer Science and Technology Department, Faculty of Chemistry, University of the Basque Country UPV/EHU, Paseo Manuel de Lardizábal, 3, 20018 Donostia-San Sebastián, Spain.

[5] IKERBASQUE, Basque Foundation for Science, Bilbao, Spain.

*corresponding authors: dario.cavallo@unige.it; alejandrojesus.muller@ehu.eus

Abstract

Three semicrystalline polyesters, poly(lactic acid), poly(caprolactone) and poly(butylene succinate) (PLA, PCL and PBS) were melt blended to prepare binary and ternary systems of selected compositions. In binary blends with a sea-island morphology, each of the polymers is either the major or dispersed phase in the various samples. Analogously, different ternary blends with a "partial-wetting" morphology are prepared, displaying droplets of PLA, PCL or PBS minor phase located at the interface between the other two major components. The crystallization behaviour of the three phases has been investigated under non-isothermal conditions via differential scanning calorimetry. In binary blends, a distinct effect of morphology on nucleation was observed, with the minor phase displaying fractionated crystallization, as a consequence of the droplet concentration being higher than that of nucleating impurities. Partially-wetting droplets of the different polymers in ternary blend show instead non-isothermal crystallization analogous to the bulk material, due to the much larger domain size. The self-nucleation behaviour of the polyesters in the binary and ternary blends

was then compared to that of the neat polymers. It was found that the very large number of self-nuclei generated by the self-nucleation protocol (in *Domain II* or self-nucleation *Domain*) applied to the samples, completely overrules any effect of blend type or composition, so that the crystallization temperature is exclusively related to the self-nucleation temperature. However, when melting memory is erased and sufficiently high melting temperatures are employed, the role of heterogeneous nucleation is apparent, and the crystallization of the given blend component is highly dependent on the particular morphology.

Keywords: Self-nucleation, ternary blends, partial-wetting, sea-island, polylactic acid, polycaprolactone, poly(butylene succinate).

1. Introduction

Among the various possible nucleation mechanisms of semicrystalline polymers, the peculiar self-nucleation process remains the least understood. The self-nucleation (SN) protocol consists in melting the polymer under "mild" conditions, i.e., relatively low temperatures and/or short times, that leads to the production of self-nuclei within the polymer melt. As a result, a large increase in nucleation density and crystallization temperature during subsequent cooling from the melt is observed. The exact nature of the residual order in the melt which provides the nucleation effect is still elusive. Blundell, Keller and Kovacs were the first to apply a self-nucleation experimental protocol to the production of single crystals with identical sizes from solution, while its first extension to Differential Scanning Calorimetry was proposed by Fillon et al. [1,2]. Müller et al. have extensively investigated self-nucleation and recently they reviewed its application to polymers, polymer blends, block and random copolymers and nanocomposites [3].

Fillon et al. [2] divided the range of self-nucleation temperatures (T_s) in three *Domains*, depending on the measured effect on re-crystallization and subsequent melting. The so-called *Domain I* (or complete melting *Domain*) is encountered when the polymer is completely molten and the crystalline memory of the material is totally erased. *Domain II* (or self-nucleation *Domain*) is entered when the applied T_s is low enough to leave self-nuclei and high enough to avoid annealing of unmolten crystals. As a consequence, the crystallization temperature of the

material will shift toward higher values during the cooling scan after self-nucleation, while no sign of melting from thickened crystals will be observed in a subsequent heating run. In *Domain III* (or self-nucleation and annealing *Domain*), the applied T_s is so low that only partial melting of the original crystals will result, and thus unmolten crystal fragments will anneal during the holding time at the specific T_s. The melting endotherm after re-crystallization will thus exhibit a sharp peak at temperatures higher than those of the non-self-nucleated material.

The issue of polymer nucleation becomes of particular interest in immiscible polymer blends containing at least one semicrystalline component. In fact, it is well known that the nucleation behaviour can be greatly affected by the blend morphology. For example, in binary blends, when the crystallizable minor component is dispersed in the form of small droplets in the continuous matrix of the major phase, fractionated crystallization can be observed. [4-14]

When the number of dispersed droplets is orders of magnitude higher than the number of heterogeneities present in the bulk polymer, the droplets are statistically free of heterogeneities and only surface or homogeneous nucleation can take place. Therefore, a single crystallization exotherm may result but at much higher supercoolings. On the other hand, when the number of droplets is equal to the number of heterogeneities present in the bulk polymer, fractionated crystallization occurs, where the crystallization of the material can occur in two or more exotherms which are related to the crystallization of different droplet populations containing heterogeneities of different nucleating efficiencies. [9,11]

On the other hand, in blends with coarser morphologies, nucleation of a semicrystalline polymer at the interface with the second immiscible component is sometime reported. [15,16] Increasing the number of the blended polymers leads to an increased morphological complexity. For ternary blends, under particular conditions of polymer interfacial tension ratios, a partial-wetting morphology can be obtained. [17-22] This morphology consists of droplets of the minor phase which are assembled at the interface of the other two major phases and display three phase contact. To date, little is known on the nucleation and crystallization of ternary blends containing one or more crystallizable component.

SN has been previously applied to several binary immiscible polymer blends characterized by a droplet-in-matrix morphology. It has been shown that self-nuclei can be injected in the polymer droplet, overcoming the effect of fractionated crystallization. For example, while an 80/20 PS/PP blend displayed four different crystallization exotherms at low temperatures when cooling from a melt in *Domain I*, a single peak at temperatures

corresponding to those of the bulk self-nucleated samples was obtained upon cooling from the lowest T_s within *Domain II*. [8] Moreover, in case two semicrystalline components in an immiscible blend show a coincident crystallization, i.e., solidify upon cooling in the same temperature range, the self-nucleation of the high-melting temperature polymer can resolve the two distinct crystallization events. [10] A similar effect has been found in double crystalline block and random copolymers. [23,24]

Despite these relevant studies, a comprehensive investigation of the effect of blend morphology on the self-nucleation behaviour of a certain semicrystalline polymer has not yet been reported. In this work, we investigated in detail immiscible ternary and binary blends of poly(lactide) (PLA), poly(ε-caprolactone) (PCL), and poly(butylene succinate) (PBS). PLA, PCL, and PBS were chosen due to their different crystallization and melting temperature ranges, this facilitates the study of the crystallization of each phase separately. All the binary blends exhibited sea-island morphology, and each polymer acted as continuous or dispersed phase in the various samples. Ternary blends showed a partial wetting morphology, with each of the three polyesters acting as minor component in the different cases. The effect of blending, composition and morphology (i.e., continuous matrix, dispersed droplets, or partially wet droplets) on the crystallization and self-nucleation behaviour of these systems will be discussed.

2. Materials and methods

2.1. Materials

Poly lactic acid (PLA) (Ingeo 3001D) was purchased from NatureWorks. PLA 3001D is a biodegradable and crystallizable grade of PLA with D isomer content of around 1.4 %. The melting point is in the range 170–180°C and the glass transition temperature (T_g) is located around 55-60°C. The polymer shows a melt flow rate (MFR) of about 22 g/10 min (210°C, 2.16 kg, D1238), a density of 1.24 g/cm^3 (D792) and a weight average molecular weight of 155,000 g/mol.

Poly(butylene succinate) (PBS) (1001MD) was purchased from Showa Denko. PBS (1001MD) is a crystallizable polymer with a melting point in the range 110-115°C and a T_g of ca. -32°C. The MFR is less than 3 g/10 min, its density is 1.26 g/cm^3, and its weight average molecular weight is 60,000 g/mol.

Polycaprolactone (PCL) (Capa™ 6800) was purchased from Perstorp. PCL Capa™ 6800 is a biodegradable polymer of MFR of 2-4 g/ 10 min, with melting point of around 58°C and T_g of ca. -65°C, a density of 1.1 g/cm^3 and a weight average molecular weight of 87,000 g/mol.

2.2. Blend preparation

The polymers were dried at 50°C under vacuum for at least 24 h before melt processing. All the blends were prepared in a Brabender internal mixer with roller rotors. The mixing was performed at 190°C and 50 rpm for 8 min. Nitrogen flow was used to purge the blends during melt mixing to minimize thermal degradation. A total of 24 g material was inserted in the mixing chamber for each blend. The samples after processing were quickly taken from the mixer and quenched in ice water to freeze-in the morphology. After drying, the blends were annealed at 185°C for 20 min under a N_2 blanket, in order to stabilize the morphology. Table 1 summarizes the compositions of the different blends.

Table 1: Composition of the prepared binary and ternary blends.

Sample	PLA wt%	PCL wt%	PBS wt%
PLA	100	-	-
PCL	-	100	-
PBS	-	-	100
PLA/PCL	90	10	-
PLA/PBS	90	-	10
PCL/PLA	10	90	-
PCL/PBS	-	90	10
PBS/PLA	10	-	90
PBS/PCL	-	10	90
PLA/PCL/PBS	45	10	45
PLA/PBS/PCL	45	45	10
PCL/PLA/PBS	10	45	45

2.3. Blend characterization

SEM analysis

The blend samples were cryo-microtomed at -150°C using a Leica instrument (RM2165) equipped with an LN21 cooling system. A desktop SEM was used to characterize the morphology at 15kV. BSE mode (image with backscattered electrons) was employed. In some cases, the samples were stained by 2 wt % phosphotungstic acid or etched by a selective

solvent to increase phase contrast. Gold coating on the microtomed surface is employed as needed.

Several micrographs of the most representative inner regions of the specimens were acquired. The diameters of the dispersed phases were then measured via image analysis. Number (*D*n) and volume (*D*v) were calculated using the following equations:

$$Dn = \sum n_i d_i / \sum n_i \qquad (1)$$

$$Dv = \sum n_i d_i^4 / \sum n_i d_i^3 \qquad (2)$$

where n_i is the number of droplets "i" of diameter D_i [7,25].

Thermal behavior of the different blends with DSC

The thermal characterization of the blends was done by Differential Scanning Calorimetry (DSC) using a Perkin Elmer DSC Pyris 1 calorimeter, equipped with a refrigerated cooling system (Intracooler 2P).

Prior to the analysis, a calibration was done using indium and tin. All measurements were performed using sample masses of approximately 5 mg and under a continuous nitrogen flow.

Non-isothermal analysis: In these measurements, the samples were first heated from room temperature to 200°C at 10°C/min and held at 200°C for 3 minutes, to erase the thermal history of all the components. The samples were then cooled at a cooling rate of 5°C/min from 200°C to −20°C, while the cooling scan was recorded. Finally, a second heating scan at a heating rate of 5°C/min was performed and acquired.

Self-nucleation experiments (SN): samples were analyzed using the self-nucleation procedure described hereinafter [2,3]:

1) Erasing the crystalline history by holding the sample in the melt at 200°C for 3 min (25°C above the melting point of the component with the higher crystallization and melting temperatures).

2) Creation of a standard crystalline state by cooling from 200°C to -20°C at a rate of 20°C/min.

3) Complete/partial melting of the sample by heating the sample at 20°C/min from -20°C to a selected temperature (T_s), where the sample was kept for 5 min. Depending on the value of T_s,

during these 5 min the sample completely melts (*Domain I*), self-nucleates (*Domain II*) or self-nucleates and anneals (*Domain III*).

4) Crystallization of the samples, thermally treated in the preceding step 3, by cooling from T_s to -20°C at a rate of 20°C/min.

5) Subsequent melting of the re-crystallized sample by heating from -20°C to 200°C at a rate of 20°C/min.

For the self-nucleation study, each sample was used for three SN temperatures only, and subsequently replaced with a fresh sample, in order to avoid the effect of possible degradation of the polymer at high temperatures on its crystallization behavior. A faster heating/cooling rate with respect to the one adopted in the non-isothermal crystallization protocol has been employed for self-nucleation experiments, in order to reduce the analysis time.

5.3. Results and discussion

Morphological characterization with Scanning Electron Microscopy analysis

Figure 1 shows SEM micrographs of cryogenically fractured surfaces of PLA/PCL/PBS, PLA/PBS/PCL, and PCL/PLA/PBS blends. It is clear that all ternary blends exhibit a partial-wetting morphology, in which the phase with the lower content (10 wt%) self-assembles into droplets located at the interface of the co-continuous structure formed by the other two major components, with a content of 45 wt% each.

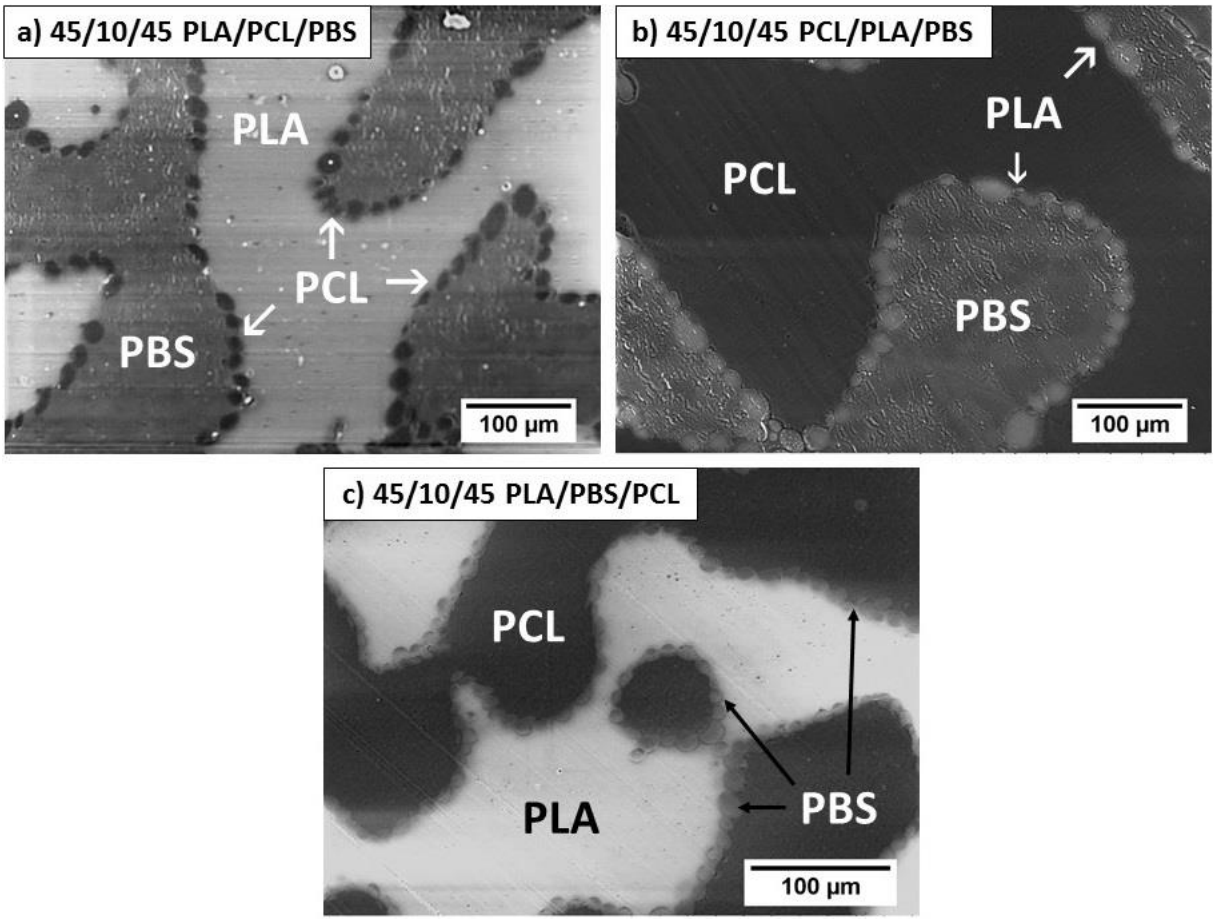

Figure 1. Morphologies of ternary blends PLA/PCL/PBS, PCL/PLA/PBS and PLA/PBS/PCL with a weight composition of 45/10/45, after annealing for 20 min at 185°C. a) and b) were directly imaged after cryo-microtoming; c) was stained by tungstic acid followed by gold coating (~1 nm thickness) before SEM analysis.

A clear phase separation was observed which confirm the immiscibility between all blend components. The obtained morphology is mainly controlled by the spreading coefficient and the interfacial tension between polymer pairs. The spreading coefficient gives the tendency of one component to spread over another component or to locate at the interface between the other two components. The exact shape of the droplets at the interface between components in different blends (45/10/45 PLA/PCL/PBS, 45/10/45 PLA/PBS/PCL, and 45/10/45 PCL/PLA/PBS) is controlled by the difference in the interfacial tension value between the middle phase and the other two surrounding components [18].

Figure 2 shows that all binary blends exhibit sea-island morphology in which the minor phase is dispersed in the form of droplets inside the matrix of the major phase. The droplets size range is from 0.5 to around 2 µm. Similarly to the morphology observed in ternary blends,

the sea-island morphology of binary blends revealed the immiscibility of the different polymer pairs. The cavities observed in different blends resulted either from the selective extraction of a given phase or from the debonding between the polymer phases during the cryogenic fracture (Figures 2c-2f). Complete debonding is a sign of immiscibility and poor adhesion between the different components in the binary blends.

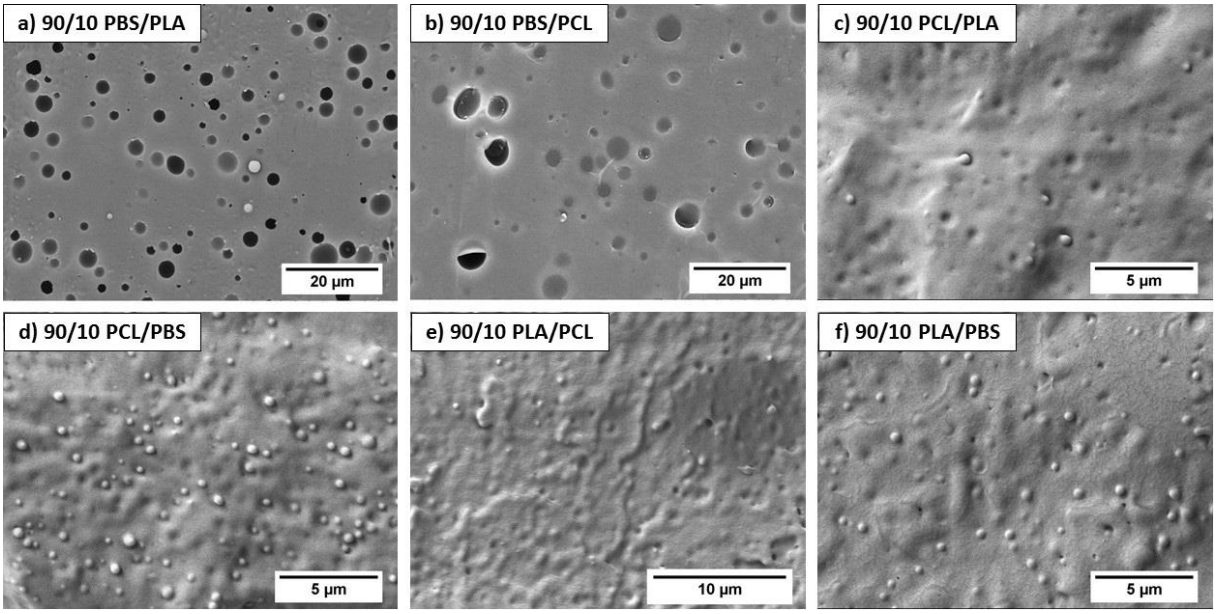

Figure 2. Morphologies of binary blends after annealing for 20 min at 185°C: a) 90/10 PBS/PLA, b) 90/10 PBS/PCL, c) 90/10 PCL/PLA, d) 90/10 PCL/PBS, e) 90/10 PLA/PCL and f) 90/10 PLA/PBS. a) and b) are cryo-microtomed samples after extraction of PLA and PCL, respectively by THF. c)-f) are cryo-fractured images without extraction.

The droplets size in binary and ternary blends has a strong effect on the crystallization behavior (temperatures and enthalpies) of the minor phase component, which leads to the appearance of the fractionated crystallization with the decrease in the droplets size, and in some cases a meaningful effect on the crystallization of the matrix component as well [4,7-14].

Table 2 reports the average particle size of the different minor phases within the blends (measured by counting at least 100 micro-domains), and the percentage of the minor phases located at the interface in the different ternary blends.

Table 2. Composition (wt%) and phase size (Number average (D_n) and volume average (D_v) diameters) of the minority phase in binary and ternary blends.

Blends	Droplet size of the minor phase (D_n/D_v) (μm)	% of the minor phase at the interface
90/10 PLA/PCL	0.41/0.54	--
90/10 PLA/PBS	0.54/0.61	--
90/10 PCL/PLA	0.45/0.55	--
90/10 PCL/PBS	0.35/0.43	--
90/10 PBS/PLA	1.4/3.6	--
90/10 PBS/PCL	1.8/5.1	--
45/10/45 PLA/PCL/PBS	21.6/28.1	95 ± 1%
45/10/45 PLA/PBS/PCL	8.3/10.1	94 ± 2%
45/10/45 PCL/PLA/PBS	24.6/32.9	98 ± 1%

DSC non-isothermal analysis

Figures 3 and 4 show DSC cooling scans and subsequent heating scans at 5°C/min for all binary and ternary blends, respectively. The thermal properties obtained during cooling and heating are separately reported in Table S1 and S2 of the Supplementary Material. The crystallization and melting enthalpies were normalized by the weight fraction of the respective component.

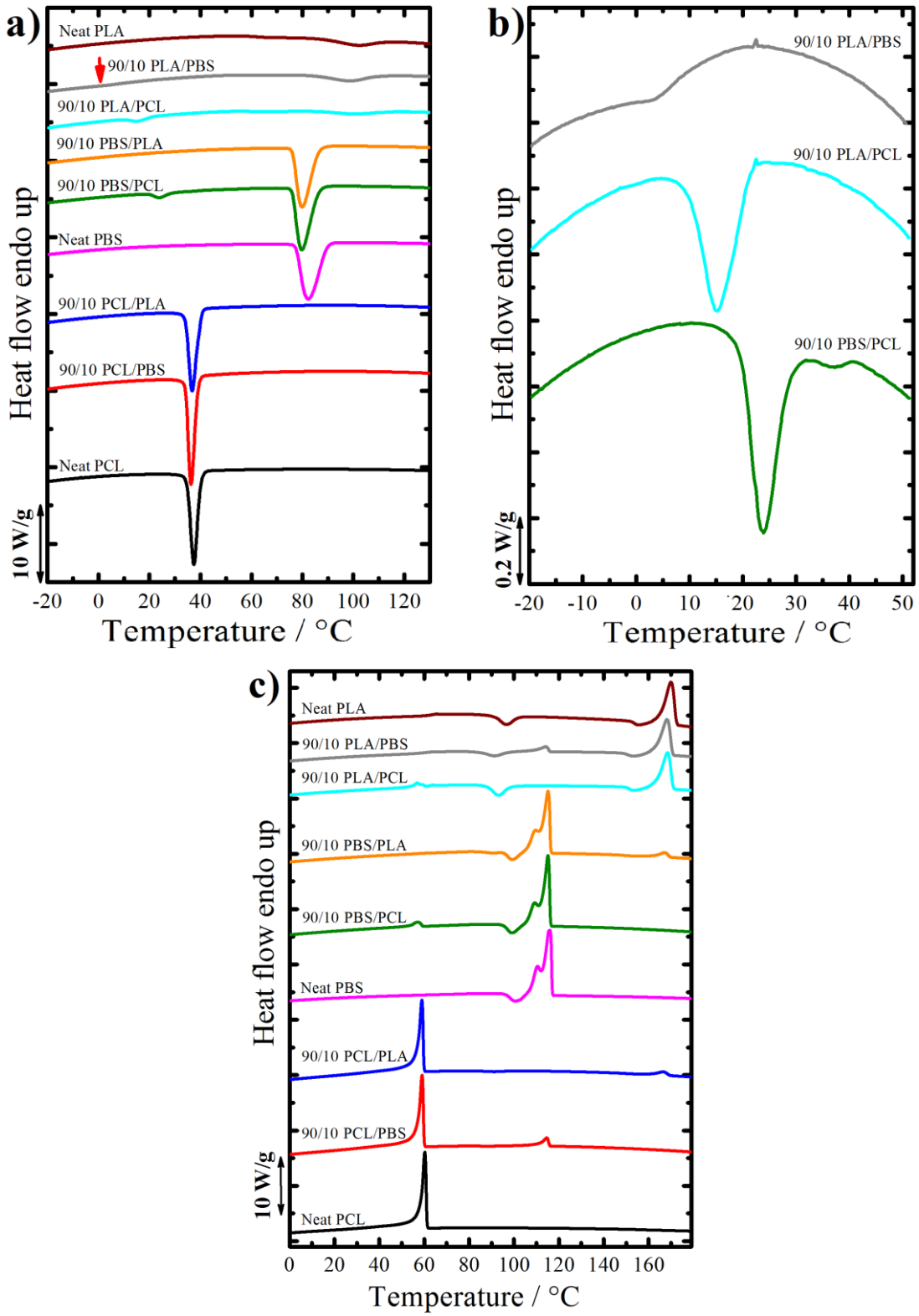

Figure 3. a) DSC cooling scans, b) zoom of the temperature region displaying weak thermal transitions upon cooling in selected samples, and c) subsequent DSC heating scans for the indicated binary blends at a cooling and heating rate of 5°C/min. The curves of neat polymers are added for the sake of comparison.

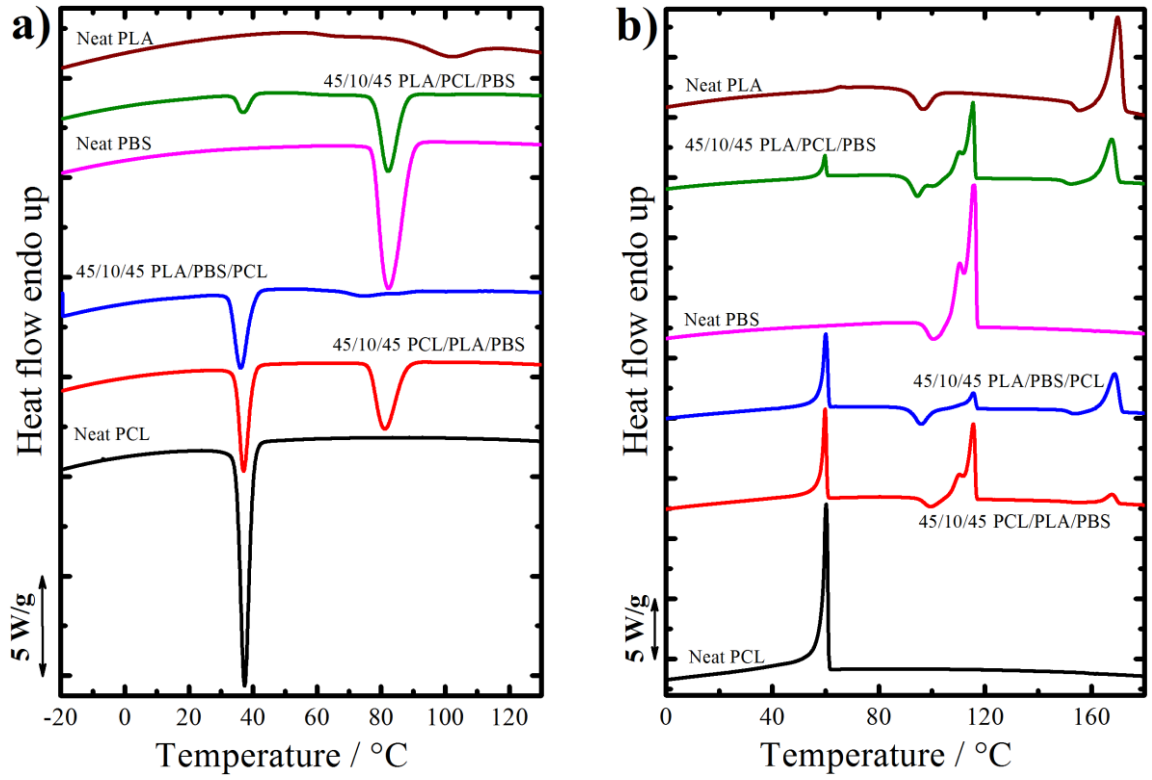

Figure 4. a) DSC cooling scans and b) subsequent DSC heating scans for the indicated ternary blends at a cooling and heating rate of 5°C/min. The curves of neat polymers are added for the sake of comparison.

At first the neat polymers are considered. Neat PBS crystallizes with a sharp peak at around 83°C, and on heating it exhibits a small cold crystallization exotherm at 100.5°C, and eventually melts at around 116°C (with a bimodal melting peak, which is probably a result of a reorganization process of the lamellae during the heating scan). PCL shows a crystallization peak at 37°C, and melts at around 61°C. Finally, PLA exhibits a broad crystallization event peaked around 101°C during cooling from the melt, a cold crystallization peak at around 97°C during heating, and a second exothermic event at about 155°C just before melting. On the basis of the literature, this peak can tentatively be attributed to the recrystallization of PLA mesophase into more stable α-crystals [26]. PLA then melts at around 170°C.

Figure 3 shows that the melt blending process affects the crystallization behavior of the different systems. Considering the crystallization of the PLA phase, in samples where this polymer is the major component, we can find a negligible shift in the crystallization peak temperature, while the crystallization enthalpy is distinctly higher in the 90/10 PLA/PBS blend with respect to the 90/10 PLA/PCL blend. Accordingly, in the heating scans (Figure 3c) a lower cold-crystallization enthalpy was obtained for PLA in the binary blend with PBS as minor

component, with respect to that with 10 wt% PCL. We can thus deduce a mild nucleating effect of the PBS phase during cooling from the melt, while the presence of PCL droplets does not significantly affect PLA major phase crystallization. The small nucleating effect can be attributed to impurity transfer from the PBS to the PLA phase, or to the effect of the PBS/PLA interfaces. Similar results of enhancement of the melt and cold crystallization rate of PLA in presence of PBS droplets were reported in literature [27-29]. Likewise, several papers reported the enhancement of the cold crystallization rate of PLA in contact with PCL droplets [25, 30-32].

When PLA is the minority component of binary blends, i.e., is present as droplets in a PCL or PBS matrix, no trace of crystallization during cooling can be observed, while a small cold-crystallization exotherm is recorded on subsequent heating. It is deduced that the concentration of PLA droplets created by blending is larger than that of the nucleating heterogeneities existing in neat PLA. As such, the nucleation of crystals is delayed and does not occur on cooling before reaching the glass transition [7,11,33-35].

Considering the crystallization of PCL, in 90/10 PCL/PLA and 90/10 PCL/PBS, the crystallization temperature keeps practically constant despite the addition of PLA or PBS. Instead, a clear reduction of the crystallization kinetics was observed for the PCL minor phase in 90/10 PLA/PCL and 90/10 PBS/PCL. The crystallization temperature of PCL decreased from 37 to around 15°C in 90/10 PLA/PCL, while the 90/10 PBS/PCL blend exhibits fractionated crystallization, with a minor peak at the same value of the neat PCL and a second crystallization event around 24°C. The depression of crystallization temperature indicates that most of the droplets contain less-active heterogeneities, and thus require a larger undercooling to crystallize at detectable rates [7]. It is worth noting that a minor fraction of PCL droplets nucleated by the same type of heterogeneities active in the neat polymer is still present in the PBS/PCL binary blend (see figure 3b).

Fractionated crystallization of PCL droplets, as described above, is a common phenomenon that is frequently seen in immiscible blends. [7-14] This behavior occurs when the number of droplets is equal or higher than the number of highly active heterogeneities present in the bulk polymer. Such highly active heterogeneities are responsible for the heterogeneous nucleation of the bulk polymer at low supercoolings. When a population of droplets does not contain these highly effective heterogeneities, it can only crystallize at higher supercoolings by nucleating onto less active heterogeneities present, or at the interface with the matrix. Homogeneous nucleation can only occur when the number of droplets exceeds by

several orders of magnitude the number of all nucleating heterogeneities present in the bulk polymer and is not normally encountered in non-compatibilized polymer blends, as droplet sizes are too large [11,36]

In the binary blends 90/10 PBS/PLA and 90/10 PBS/PCL, the crystallization temperature of PBS was slightly decreased from 82.5°C to 80°C, possibly due to some impurity transfer from PBS to the other phases during melt processing. When PBS forms dispersed droplets, it exhibits slower crystallization. In 90/10 PLA/PBS the crystallization temperature decreased to around 3°C (see figure 3b), while in 90/10 PCL/PBS, the crystallization of PBS droplets appeared to be concomitant with the crystallization of PCL matrix, peaked at 36.5°C. This deduction will be confirmed later on by applying the self-nucleation protocol.

At this stage, the crystallization behavior of the various components in ternary blends is considered. Figure 4a shows the DSC cooling scan of neat components and ternary blends: it is clear that melt blending does not affect significantly the crystallization behavior of both PCL and PBS in all the ternary blends. On the other hand, no trace of PLA crystallization could be detected in 45/10/45 PLA/PCL/PBS and 45/10/45 PCL/PLA/PBS ternary blends, suggesting a possible transfer of nucleating impurities from PLA to the other molten phases during mixing. Instead, PLA crystallizes on cooling to a certain extent in the ternary blend 45/10/45 PLA/PBS/PCL.

The DSC heating scans of the different homopolymers and ternary blends are reported in Figure 4b. No significant changes of the PCL and PBS melting temperatures and enthalpies was observed, while the cold crystallization temperature of the PLA component is slightly decreased in both blends with respect to the one of the homopolymer, suggesting a possible mild nucleating effect of PBS and/or PCL. We note that the cold crystallization enthalpy of PLA in the ternary blends is not measurable, due to the overlap with the PBS melting peak.

Contrary to what has been observed in binary blends, fractionated crystallization of the minor phases has not been observed in ternary blends. The different behavior can be attributed to the large droplet size difference, as highlighted in Table 2. In particular, the average size of the minor phase domains increased from around 1 μm in binary blends to around 20 μm in ternary blends, for all the considered polymers. The larger droplet size in ternary blends results in a higher opportunity of finding highly active nucleating heterogeneity inside the minor phase, which in turns leads to its crystallization at supercoolings similar to those detected for the neat homopolymers.

The data presented in Figures 3 and 4, revealed that the variation in the droplets sizes (Table 2) of the different dispersed phase does not significantly affect the crystallization behavior of the various components.

Self-nucleation

Self-nucleation of PLA in 90/10 PLA/PCL blend:

Figure 5 shows DSC cooling and heating runs after self-nucleation of the PLA phase at different T_s values. Under normal conditions, i.e., heating the sample into *Domain I*, PLA shows an almost negligible trace of crystallization trace during cooling (around 100°C), while it undergoes extensive cold crystallization upon subsequent heating. By applying SN, the crystallization rate of the self-nucleated PLA increases noticeably.

At temperatures higher than 170°C (*Domain I*), no changes in the cooling and/ melting behaviors of PLA can be observed. When the employed T_s is in the range 170-169°C (*Domain II*), a clear PLA crystallization exotherm appeared in the DSC cooling scan, and the subsequent cold-crystallization decreases accordingly. Within *Domain II*, the decrease in the employed T_s results in a large increase in the crystallization temperature and enthalpy (Figure 5a). Further decreases in T_s to temperatures lower than 168°C resulted in an additional enhancement in the crystallization behavior. In particular, two distinct crystallization events appear on cooling, with the relative fraction of the higher temperature one becoming larger with decreasing T_s (Figure 5a). In agreement with this enhanced crystallization, no cold-crystallization exotherm was observed on subsequent heating.

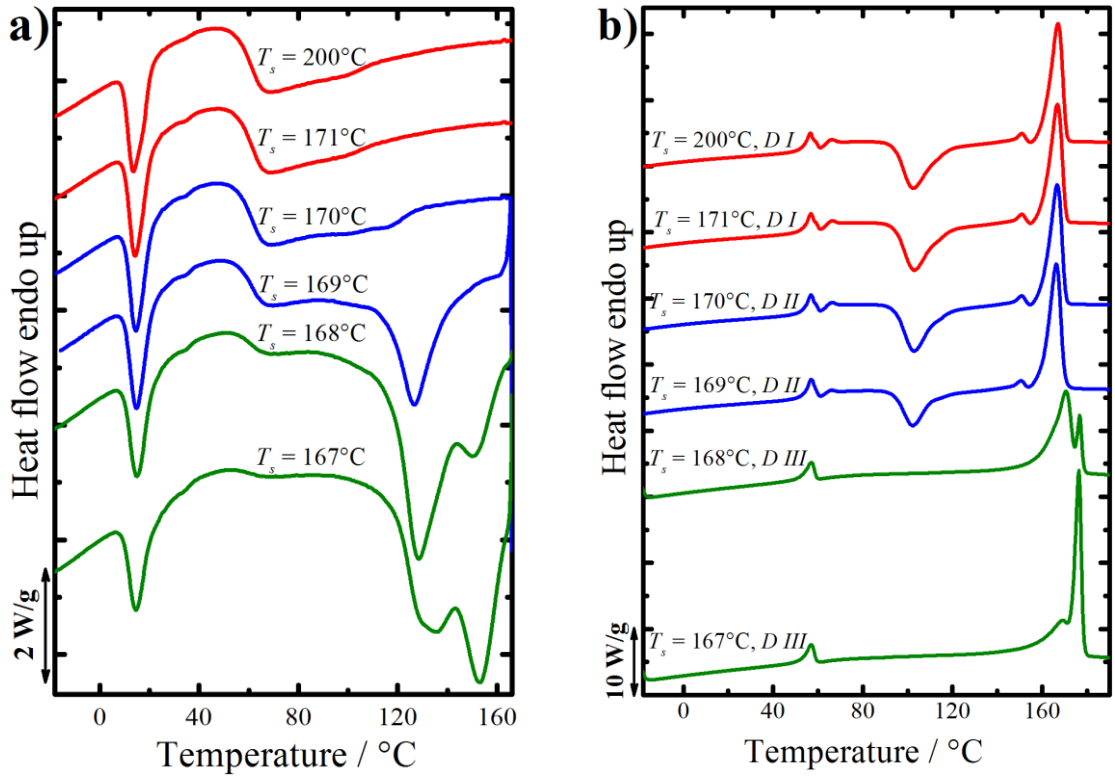

Figure 5. a) DSC cooling scans (at 20°C/min) for 90/10 PLA/PCL blend after 5 min at the indicated T_s. (b) Subsequent heating scans (at 20°C/min) after the cooling runs shown in (a).

Moreover, the step increase in heat capacity associated with the glass transition of amorphous PLA, which in samples self-nucleated at higher temperatures occurred around 65°C, although partially superposed to the melting endotherm of the PCL minor phase, could not be clearly detected (Figure 5b)and is apparent on cooling only (Figure 5a). Finally, a sharp annealing peak at higher temperatures in the melting scan appears, allowing the detection of *Domain III*.

The three self-nucleation *Domains* of PLA within the 90/10 PLA/PCL binary blend are summarized in Figure S1 (Supplementary Material file), where the crystallization temperature at the different T_s are superposed to a standard DSC melting endotherm of PLA. The transition between *Domain I* and *Domain II* is practically coincident with the melting endotherm endpoint.

Self-nucleation of PCL in 90/10 PBS/PCL blend:

Figure 6a shows the DSC cooling curves after self-nucleating the PCL minor phase at different T_s. It should be noted that due to the relatively small T_s values employed to SN the PCL phase, Figure 6 only plots a limited temperature range, hence the PBS phase melting cannot be observed when a T_s value of 140°C was employed.

As a consequence of melt blending, the PCL phase within 90/10 PBS/PCL undergoes fractionated crystallization showing two crystallization peaks (at around 31 and 22°C), corresponding to two populations of PCL droplets containing nucleating heterogeneities with different efficiencies. The SN protocol causes the injection of self-nuclei into PCL droplets. By decreasing T_s within *Domain II*, the enthalpy of the low-temperature crystallization peak decreases, while the opposite occurs to the high-temperature crystallization event. Also, a shift of the major crystallization peak towards higher temperature is observed. The annealing at T_s causes the appearance of a small endothermic signal above the melting point of PCL crystals, which is associated to an annealing peak of the PBS matrix. This can be confirmed in separate experiments, where the same annealing is applied, but avoiding the crystallization step of the PCL phase (see Figure S2 in the Supplementary Material).

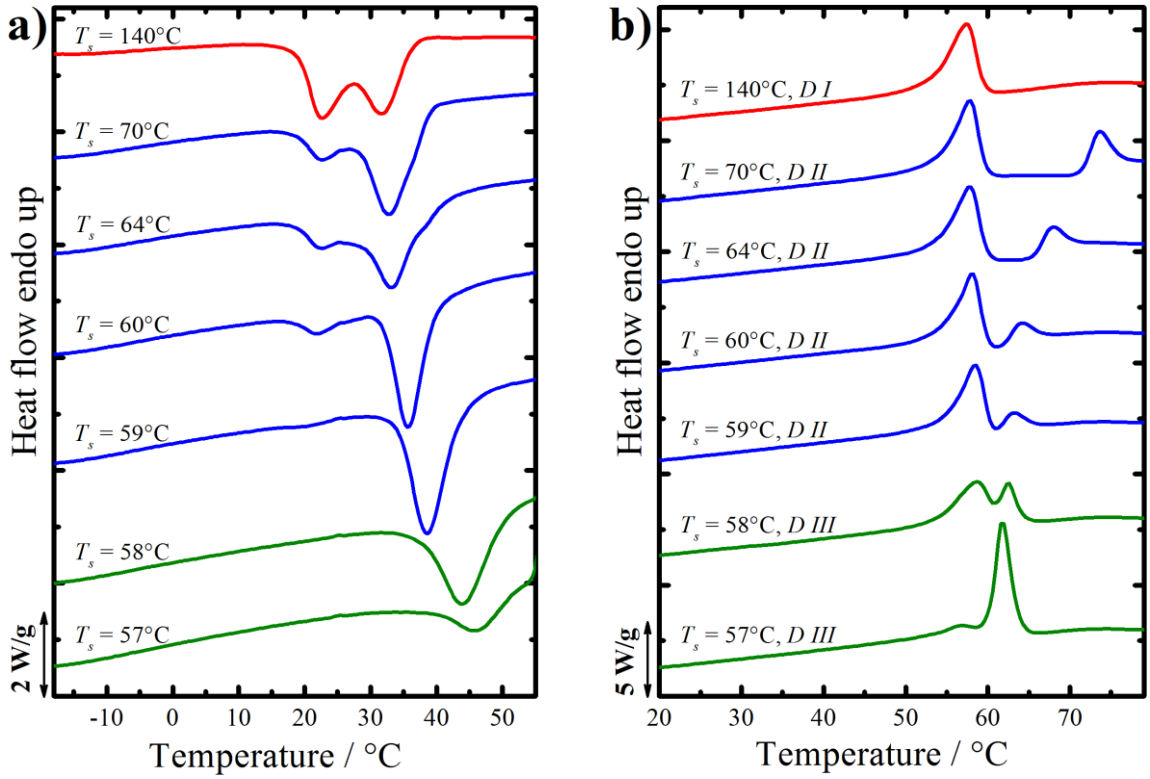

Figure 6. a) DSC cooling scans (at 20°C/min) of 90/10 PBS/PCL blend after 5 min at the indicated T_s. (b) Subsequent heating scans (at 20°C/min) after the cooling runs shown in (a).

At temperatures equal to or lower than 58°C all the droplets are self-nucleated (as judged by the disappearance of the low-temperature exotherm), and *Domain III* is found. In fact, a sharp peak related to the high melting-temperature annealed PCL crystals is observed, although probably partially superposed with the PBS low-temperature endotherm. PCL displays a strong crystalline memory effect: *Domain II* extends to T_s = 71°C, i.e., 10°C above the standard melting endpoint (Figure S3, Supplementary Material). The strong crystalline memory of PCL

at temperatures distinctly higher than its melting point was recently investigated by means of rheological and dielectric spectroscopy measurements. [37,38]

Self-nucleation of PBS in 90/10 PCL/PBS blend

Self-nucleation can also be used to separate the "coincident crystallization" of double crystalline polymer blends. Coincident crystallization occurs when the two crystalline components of a blend displaying sea-islands morphology crystallize concurrently in the same temperature range. Typically, once the crystallization of the matrix starts, it is quickly followed by the crystallization of the dispersed droplets, nucleated by the crystalline matrix. Therefore, DSC cooling scans shows a single crystallization peak, while two separate melting peaks associated with the melting of each component are observed in the subsequent heating scan. The presence of coincident crystallization phenomena can be revealed by WAXS and/or self-nucleation techniques [3,4,7,23,24,39-41].

Figure 7a and 7c show the DSC cooling and heating scans of 90/10 PCL/PBS self-nucleated at different T_s, between 140°C and 110°C, while Figures 7b and 7d show a close-up on PBS crystallization and melting temperature ranges.

At T_s higher than 118°C, a single crystallization peak around 35°C can be observed, but upon heating both PCL and PBS phase melting peaks are clearly revealed, indicating that coincident crystallization of both polymers took place during the cooling scan.

For lower self-nucleation temperatures, in the range 118-116°C, two crystallization peaks located between 65-100°C appear (see Figure 7b). These exothermic peaks can be related to the crystallization of different populations of PBS droplets. Simultaneously, the crystallization enthalpy of the main peak around 35°C decreases from 56 J/g at T_s = 140°C to 53 J/g at T_s 116°C (not shown). This small decrease is an indirect proof of the obtained separation between PBS and PCL crystallization events. Below T_s =116°C, PBS crosses into *Domain III*, and the further increase in the crystallization temperature is associated to the emergence of PBS annealing peaks with high melting temperature (see Figures 7c and 7d). We note that *Domain II* in this system starts only slightly above the end of the melting endotherm of PBS (Figure S4, Supplementary Material), however, the self-nucleation effect is dramatic, since the crystallization temperature shifts from below 40°C (coincident with PCL major phase)

for *Domain I*, to above 70 and 90°C. The obtained results demonstrate the efficiency of SN protocol in separating coincident crystallization phenomena.

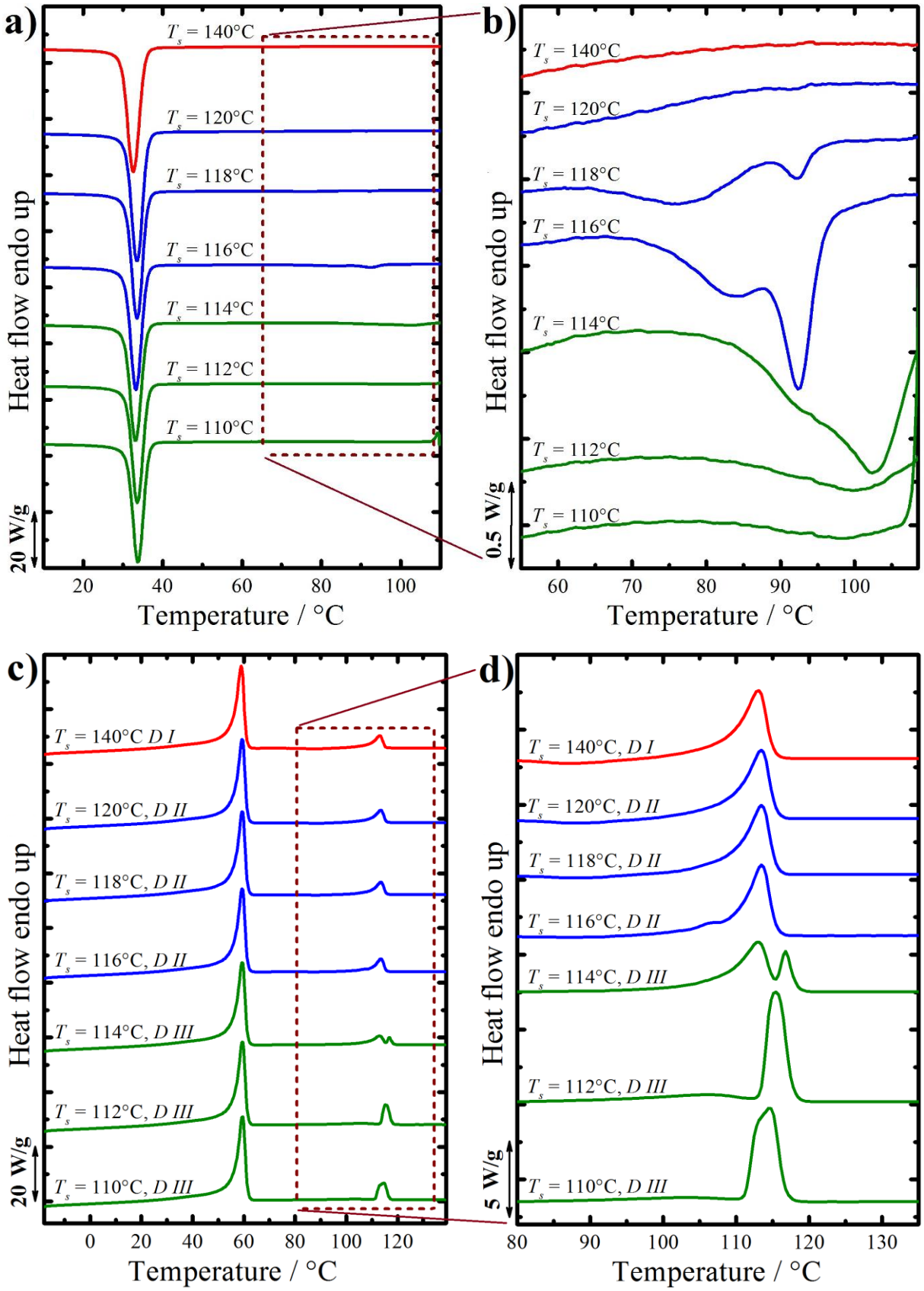

Figure 7. a) DSC cooling scans (at 20°C/min) of 90/10 PCL/PBS blend after 5 min at the indicated T_s; (b) is a close-up of the PBS crystallization temperature range; (c) Subsequent heating scans (at 20°C/min) after the cooling runs shown in (a); (d) is a close-up of the PBS melting temperature region.

In the following, the self-nucleation behavior of the minor components, located at the interface between the two major phases in the ternary blends, is analyzed and compared to that of binary blends and neat polymers.

Self-nucleation of PLA in 45/10/45 PCL/PLA/PBS blend

Figures 8a through 8d show the crystallization and melting behavior of 45/10/45 PCL/PLA/PBS ternary blends upon cooling and subsequent heating from different self-nucleation temperatures, with emphasis on the PLA phase. By employing self-nucleation temperatures higher than 170°C, no changes are found in the cooling or re-heating scans, a behavior characteristic of *Domain I*. Upon decreasing T_s, the crystallization process of PLA is enhanced, and *Domain II* is encountered. In particular, a small exothermic peak around 125°C can be found during cooling from T_s = 169°C, while the crystallization of PLA from T_s = 170°C cannot be directly detected. Nevertheless, the bimodal melting endotherm on subsequent heating suggests a different crystallization process with respect to higher self-nucleation temperatures. Therefore, T_s = 170°C can be tentatively attributed to *Domain II*. *Domain III* is found for self-nucleation temperatures equal or lower than 168°C. Next to the main crystallization event, a second small exotherm at higher temperatures appears in the cooling scan, possibly related to the nucleation effect of annealed crystal fragments (Figure 8b). The presence of such crystals is detected on subsequent heating, as evidenced by a relatively sharp melting peak around 175°C. The width of *Domain II* for the PLA phase in the ternary blend is only about 2 Celsius degrees, partially superposed with the high temperature tail of the standard melting endotherm (Figure S5, Supplementary Material file).

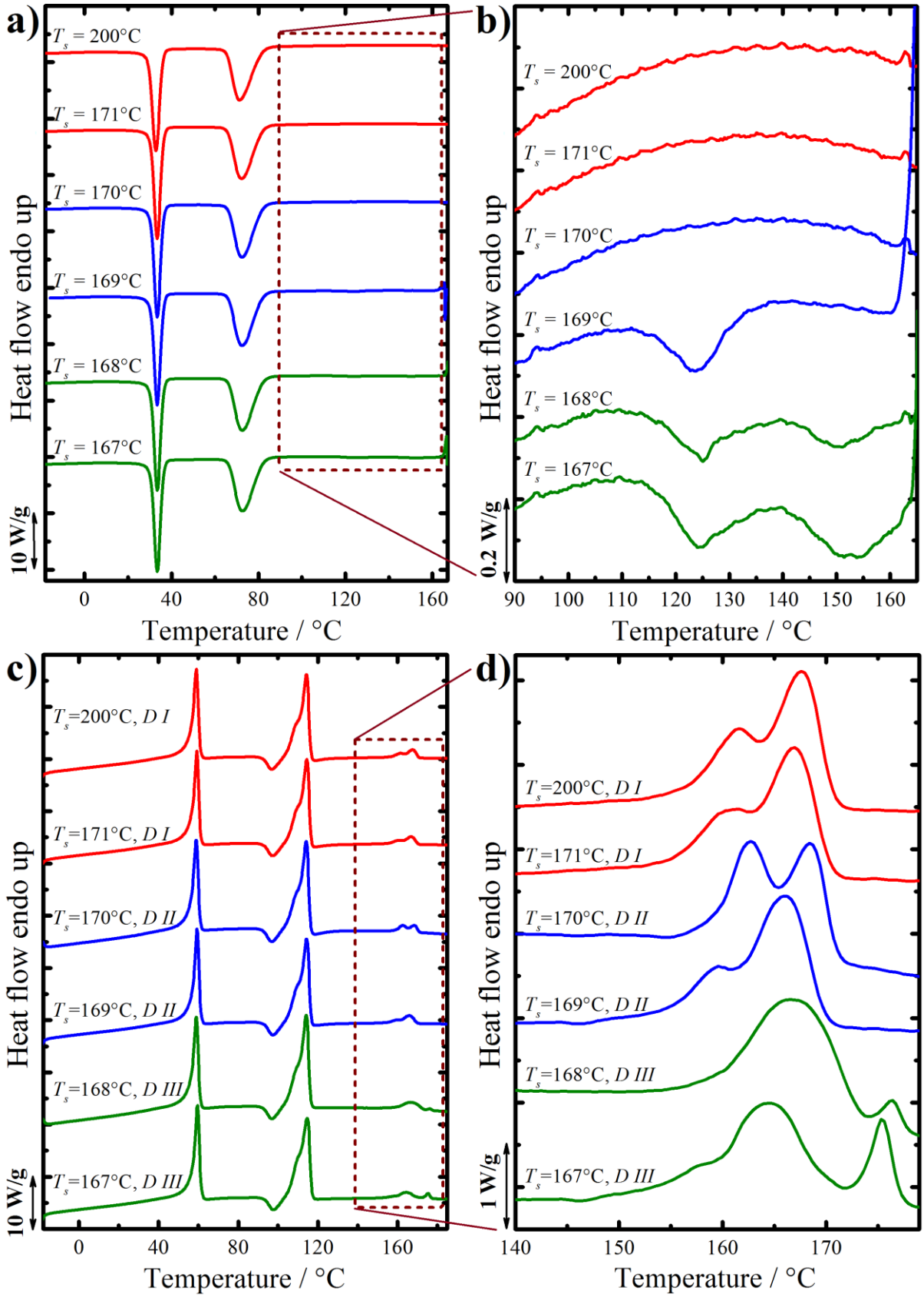

Figure 8. a) DSC cooling scans (at 20°C/min) for 45/10/45 PCL/PLA//PBS blend after 5 min at the indicated T_s; (b) Close-up of the PLA crystallization temperature region; (c) Subsequent

heating scans (at 20°C/min) after the cooling runs shown in (a); (d) Close-up of the PLA melting temperature region.

Self-nucleation of PBS in 45/10/45 PLA/PBS/PCL

The results on the behavior of PBS droplets at the interface with PLA and PCL *Domains* are reported in Figure 9 for various self-nucleation temperatures.

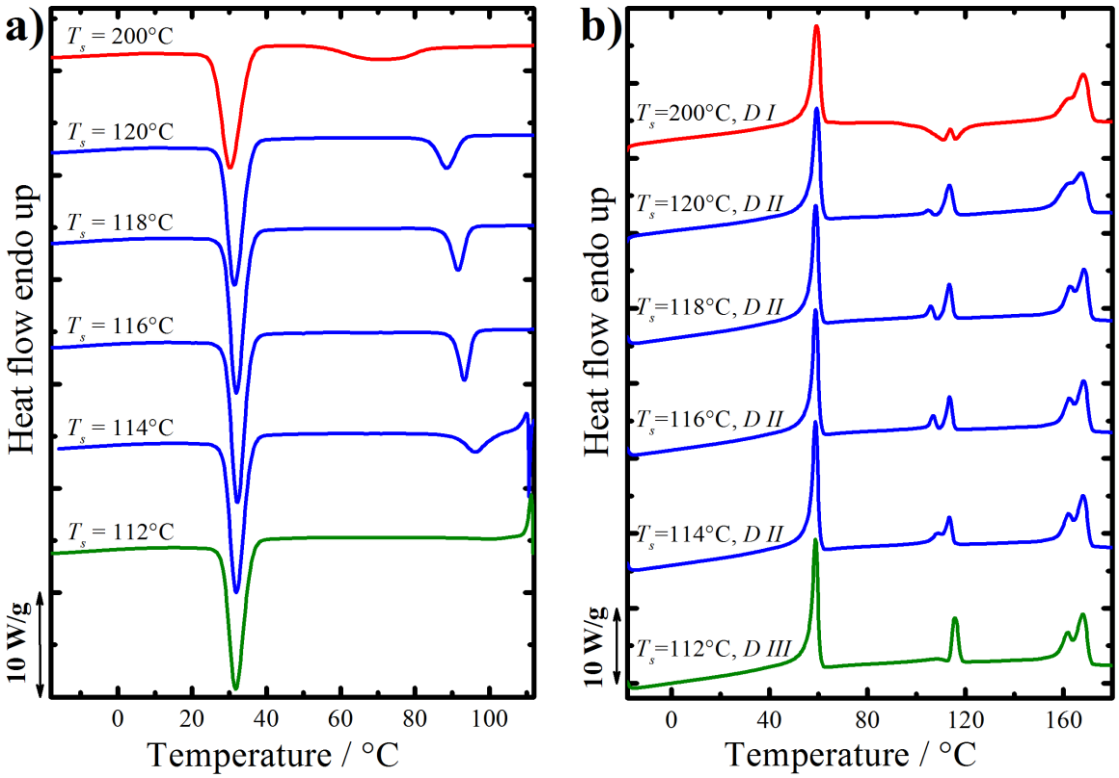

Figure 9. a) DSC cooling scans (at 20°C/min) for 45/10/45 PLA/PBS/PCL blend after 5 min at the indicated T_s; (b) Heating scans (at 20°C/min) after the cooling runs shown in (a).

Crystallization of PBS occurs slowly during cooling from the melt (i.e., in *Domain I*, see Figure 9a, cooling DSC scan from T_s =140°C) resulting in a broad exotherm. Under this cooling condition, PLA crystallization is bypassed, and it can only crystallize upon subsequent heating, in a temperature range which is superposed on the melting of PBS crystals (Figure 9b). The lowest self-nucleation temperature (i.e., in *Domain II*) probed, T_s =120°C shows already a clear signature of enhanced PBS crystallization. The crystallization peak is shifted to temperatures higher than 15°C than those typical of *Domain I* crystallization, and displays a sharper appearance. In addition, no trace of PLA cold-crystallization is observed in the subsequent heating step.

The PBS crystallization temperature (Figure 9a) continues to increase upon lowering T_s, without apparent changes in the melting behavior, down to a self-nucleation temperature of 116°C (*Domain II*, see Figures 9a and 9b). For lower self-nucleation temperatures, *Domain III* is entered as judged by the reduction in crystallization enthalpy upon cooling and by the changes in the shape of the subsequent PBS melting endotherm. Although we did not investigate in detail the onset of the self-nucleation *Domain* (i.e., the *Domain I/Domain II* transition temperature), it is already clear that the crystalline memory effect extends well above the end of the melting endotherm (Figure S6 Supplementary Material), similarly to what is typically found for the neat polymer [24]

Self-nucleation of PCL in 45/10/45 PLA/PCL/PBS

The self-nucleation of PCL droplets at the interface with solid PLA and PBS phases is analyzed in Figures 10a through 10d. The behavior is analogous to that previously shown in PBS/PCL binary blend. A distinct self-nucleation effect can be deduced for T_s lower than about 70°C (*Domain II*, see Figure 10a). The exact identification of *Domain III*, from the melting trace after re-crystallization (Figures 10b and 10c) is complicated by the concomitant occurrence of an endothermic effect (annealing peak or aging of the rigid amorphous fraction [42-44]) related to the PBS phase, just slightly above the melting peak of PCL (see also Figure 6 and S2). Tentatively, the melting of annealed PCL crystals can be distinguished from the PBS-related endotherm at T_s equal or lower than 58°C, when the PBS signal becomes weaker while the peak attributed to PCL gets sharper. The relatively strong memory effect of PCL is confirmed also for this blend, since the fully relaxed *Domain I* is obtained only at temperatures well above the end of the crystals melting endotherm (Figure S7, Supplementary Material).

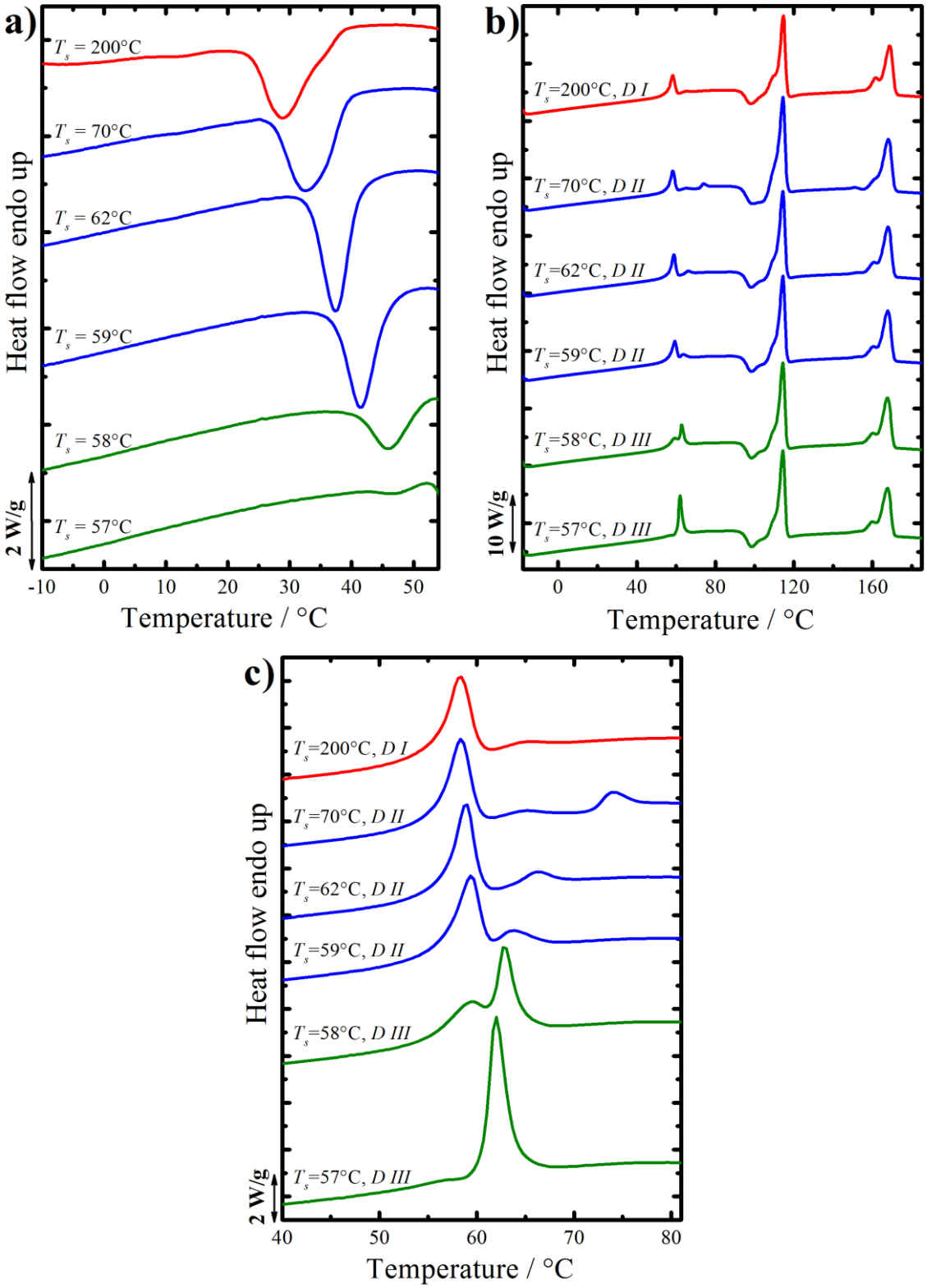

Figure 10. a) DSC cooling scans (at 20°C/min) for 45/10/45 PLA/PCL/PBS blend after 5 min at the indicated T_s; (b) Heating scans (at 20°C/min) after the cooling runs shown in (a); (c) Close-up of the PCL melting temperature region

Finally, the self-nucleation behavior of the different polymers in the various blends is compared in Figures 11a through 11c. As a general remark, we note that the boundaries between the self-nucleation *Domains* are basically unaffected by the blending process, or at most they vary by about 1 or 2 Celsius degrees. Moreover, the T_c values of self-nucleated samples at the same temperature within *Domain II* are remarkably similar, notwithstanding the phase content in the blend or the blend type (binary vs. ternary). This is true for all the three polymers, but is particularly evident for PLA and PBS phases.

We can deduce that the production of self-nuclei is mainly determined by the T_s temperature with no significant influence of blend morphology. This can be interpreted considering the exceedingly high number of self-nuclei that can be injected into the system, in comparison to the number of existing nucleating impurities or interfaces in the blend. Typically, the self-nucleation process is capable of introducing approximately 10^{12} to 10^{13} self-nuclei at the ideal self-nucleation temperature (i.e., the lowest temperature in *Domain II*, where the maximum number of self-nuclei are produced) [2,3]. PCL is the polymer with the highest heterogeneous nucleation density in the bulk, as compared to PBS and PLA, as judged by the typical spherulitic size upon cooling from the melt (data not shown). In the case of bulk PCL, the maximum heterogeneous nucleating density has been estimated by polarized optical microscopy to be of the order of 10^6-10^8 nuclei/cm^3. This means that SN of PCL can enhance its nucleation density by 4-7 orders of magnitude. In the cases of PBS and PLA the enhancement would be even larger [45,46].

On the other hand, self-nucleation temperatures within *Domain I* reveal morphology-related differences in T_c, since the intrinsic nucleation behavior of the particular blend is exposed. We note that the data reported in Figure 11 differ from those discussed in Tables S1 and S2 and Figures 3 and 4, due to the different cooling rate employed (i.e., 20 vs. 5°C/min).

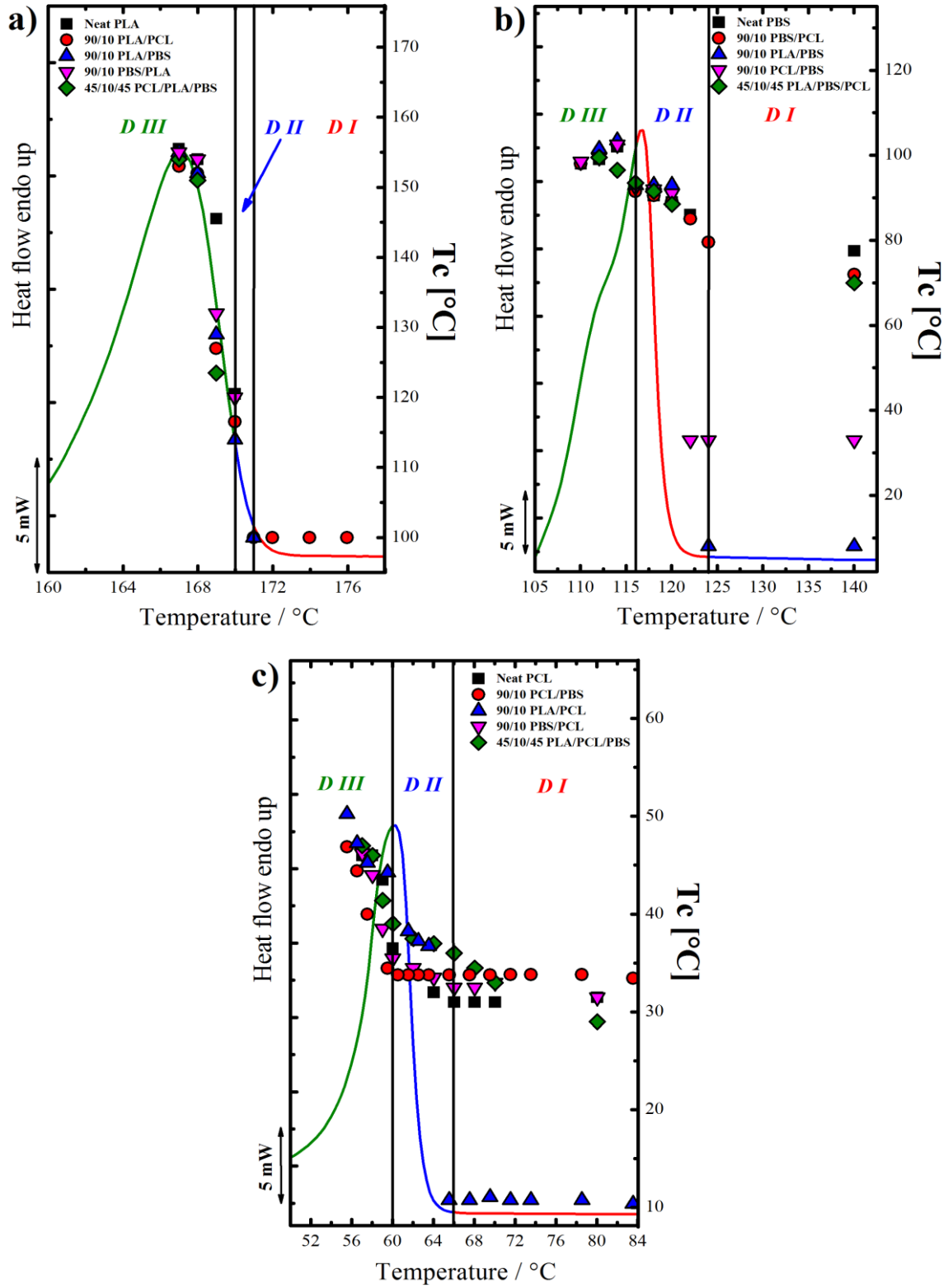

Figure 11. Collection of T_c as a function of the employed T_s for (a) PLA, (b) PBS and (c) PCL in different blends and neat components. The data are superposed to standard melting curves of the relative polymer and the boundaries between SN *Domains* in the neat polymer are also indicated.

For what concerns the PLA phase, crystallization can be inhibited at 20°C/min for the neat polymer, as well as for binary and ternary blends with a minor fraction of this component (see Figure 11a). Interestingly, for binary blends with PBS or PCL where PLA is the matrix, a different behavior is observed. The 90/10 PLA/PCL blend can crystallize to a certain extent upon cooling at 20°C/min, while the same does not occur in the 90/10 PLA/PBS blend. This enhanced crystallization can be due the different nucleating impurities that have been transferred to the PLA matrix in the two cases, or to a higher nucleation efficiency at the interface with molten PCL droplets, with respect to molten PBS. It should also be considered that PBS droplets in this blend have a high tendency to coalesce during melting, contrary to PCL ones. As such, the small differences in the nucleating effect towards PLA between the two molten polymers can be enhanced by the much higher amount of PCL surface per unit volume of blend, due to the smaller droplet size after melting for some time.

In the case of PBS, crystallization at temperatures equivalent to those of the neat polymer occurs in *Domain I* for binary blends where PBS is the major component, as well as in ternary blends where PBS forms (relatively large) droplets at the interface between PLA and PCL. However, crystallization is depressed in the binary blend with 10 wt% PBS (Figure 11b). Among the two blends (90/10 PLA/PBS and 90/10 PCL/PBS), the one with PCL as major phase shows the faster kinetics. This is attributed to differences in the transfer of nucleating impurities between the polymers during blending. Furthermore, the possible nucleating action of crystalline PLA on molten PBS, might be inactive given the fact that PLA is not able to crystallize at the applied cooling rates.

Finally, in the case of PCL, only minor differences between the crystallization of the neat polymer, the ternary blend with PCL concentration of 10% and the two binary blends (90/10 PBS/PCL and 90/10 PCL/PBS) could be observed (Figure 11c). In particular, by comparing neat PCL and 90/10 PCL/PBS blends, a small nucleating effect of PBS droplets on the PCL matrix can be noticed, and it can be attributed to the crystallization of PBS phase which induces the coincident crystallization of PCL matrix. On the other hand, PCL droplets in 90/10 PLA/PCL binary blend crystallize at much larger undercoolings with respect to those in 90/10 PBS/PCL blend. This difference of about 20 Celsius degrees can be tentatively ascribed to the nucleating effect of crystalline PBS or to the differences in droplet size between the two blends, given the much larger volume-averaged diameter of PCL domain size in the PBS/PCL blend (see Table 2).

4. Conclusions

In this work, we focused on triple-crystalline thermoplastic polyester immiscible blends. The crystallization of these complex materials greatly depends on their morphology, as determined by their composition and thermal history. Two different kinds of blend morphology were successfully produced, namely a sea-island morphology in binary blends and a partial-wetting morphology in the ternary blends.

For binary blends, the crystallization behavior was investigated by DSC, revealing enhanced or depressed crystallization of a given polymer in the different blends. In particular, a small acceleration of PLA cold-crystallization by both PCL and PBS phases was observed, while slower crystallization kinetics for the dispersed phase was reported for all polymers.

The self-nucleation behavior of the different polymers in the various blends was also studied. It was found that the crystallization temperatures of samples self-nucleated at the same temperature are remarkably similar, notwithstanding the phase content in the blend or the morphology. As a consequence, the boundaries between different self-nucleation *Domains* are also basically unaffected by the blending process, or at most they vary by less than 2 Celsius degrees. This is true for all the three polymers, allowing us to deduce that the production of self-nuclei is mainly determined by the self-nucleation temperature, with only a negligible influence of blend morphology and polymer content. This is attributed to the exceedingly high number of self-nuclei produced by SN, in comparison to the number of existing nucleating impurities or interface-induced nuclei. In fact, when T_s temperatures within *Domain I* are employed (i.e., no self-nucleation), the influence of heterogeneous nucleation is highlighted, in particular for minor components in blends with sea-island morphology.

5. Acknowledgements

S.E.F., A.J.M. and D.C. would like to acknowledge funding from the project H2020-MSCA-RISE-2017-778092 « BIODEST ». On the occasion of this special issue, A.J.M. and D.C would like to express their deep appreciation for the work of Christoph Schick, which has greatly contributed to fast chip calorimetry and to a deeper understanding of polymer crystallization. A.J.M. and D.C. are also thankful to Christoph Schick for the many insightful

discussions throughout the years, in particular during the various successful « Laehnwitzseminar » they attended.

6. References

1. Blundell DJ, Keller A, Kovacs AJ (1966) A new self-nucleation phenomenon and its application to the growing of polymer crystals from solution. J Polym Sci B Polym Lett. 4:481–486
2. Fillon B, Wittmann JC, Lotz B, Thierry A (1993) Self -Nucleation and Recrystallization of isotactic Polypropylene (α Phase) Investigated by Differential Scanning Calorimetry. J. Polym. Sci., Part B: Polym. Phys. 31:1383-1393
3. Michell RM, Mugica A, Zubitur M, Müller AJ (2017) Self-Nucleation of Crystalline Phases Within Homopolymers, Polymer Blends, Copolymers, and Nanocomposites. Adv Polym Sci. 276:215-256
4. Müller AJ, Michell RM (2016) Differential Scanning Calorimetry of Polymers. In: Guo Q (ed) Polymer Morphology: Principles, Characterization, and Processing. John Wiley & Sons, Inc., New Jersey, p 72-99
5. Utracki LA, Wilkie C (Eds) (2014) Polymer Blends Handbook. Springer, New York
6. Paul DR, Barlow JW (1980) Polymer Blends (or Alloys). J. Macromol. Sci., Rev. Macromol. Chem. Phys. 18:109-168
7. Arnal ML, Matos ME, Morales RA, Santana OO, Müller AJ (1998) Evaluation of the fractionated crystallization of dispersed polyolefins in a polystyrene matrix. Macromol. Chem. Phys. 199:2275-2288
8. Arnal ML, Müller AJ (1999) Fractionated crystallisation of polyethylene and ethylene/a-olefin copolymers dispersed in immiscible polystyrene matrices. Macromol. Chem. Phys. 200:2559-2576
9. Santana OO. Müller AJ (1994) Homogeneous nucleation of the dispersed crystallizable component of immiscible polymer blends. Polym. Bull. 32:471-477
10. Morales RA, Arnal ML, Müller AJ (1995) The evaluation of the state of dispersion in immiscible blends where the minor phase exhibits fractionated crystallization. Polym. Bull. 35:379-386

11. Michell RM, Blaszczyk-Lezak I, Mijangos C, Müller AJ (2013) Confinement effects on polymer crystallization: From droplets to alumina nanopores. Polymer. 54:4059-4077
12. Tol RT, Mathot VBF, Groeninckx G (2005) Confined crystallization phenomena in immiscible polymer blends with dispersed micro- and nanometer sized PA6 droplets, part 2: reactively compatibilized PS/PA6 and (PPE/PS)/PA6 blends. Polymer. 46:383-396
13. Tol RT, Mathot VBF, Groeninckx G (2005) Confined crystallization phenomena in immiscible polymer blends with dispersed micro- and nanometer sized PA6 droplets, part 3: crystallization kinetics and crystallinity of micro- and nanometer sized PA6 droplets crystallizing at high supercoolings. Polymer. 46:2955-2965
14. Yordanov C, Minkova L (2005) Fractionated crystallization of compatibilized LDPE/PA6 blends. Eur. Polym. J. 41:527–534
15. Pan P, Shan G, Bao Y (2014) Enhanced Nucleation and Crystallization of Poly(L-lactic acid) by Immiscible Blending with Poly(vinylidene fluoride). Ind. Eng. Chem. Res. 53:3148-3156
16. Kong Y, Ma Y, Lei L, Wang X, Wang H (2017) Crystallization of Poly(ϵ-caprolactone) in Poly(vinylidene fluoride)/Poly(ε -caprolactone) Blend. Polymers 9:42
17. Virgilio N, Marc-Aurèle C, Favis BD (2009) Novel Self-Assembling Close-Packed Droplet Array at the Interface in Ternary Polymer Blends. Macromolecules. 42:3405-3416
18. Ravati S, Favis BD (2013) Tunable morphologies for ternary blends with poly(butylene succinate): Partial and complete wetting phenomena. Polymer. 54:3271-3281
19. Zolali AM, Favis BD (2016) Partial and Complete Wetting in Ultralow Interfacial Tension Multiphase Blends with Polylactide. J. Phys. Chem. B. 120:12708-12719
20. Zolali AM, Favis BD (2017) Partial to complete wetting transitions in immiscible ternary blends with PLA: the influence of interfacial confinement. Soft Matter. 13:2844-2856
21. Virgilio N, Desjardins P, L'Espérance G, Favis BD (2009) In Situ Measure of Interfacial Tensions in Ternary and Quaternary Immiscible Polymer Blends Demonstrating Partial Wetting. Macromolecules. 42:7518-7529
22. Zolali AM, Favis BD (2017) Compatibilization and toughening of co-continuous ternary blends via partially wet droplets at the interface. Polymer 114:277-288
23. Müller AJ, Albuerne J, Márquez L, Raquez JM, Degée Ph, Dubois Ph, Hobbs J, Hamley IW (2005) Self-nucleation and crystallization kinetics of double crystalline poly(p-dioxanone)-b-poly(ε-caprolactone) diblock copolymers. Faraday Discuss. 128:231-252

24. Arandia I, Mugica A, Zubitur M, Arbe A, Liu G, Wang D, Mincheva R, Dubois Ph, Müller AJ (2015) How Composition Determines the Properties of Isodimorphic Poly(butylene succinate-ran-butylene azelate) Random Biobased Copolymers: From Single to Double Crystalline Random Copolymers. Macromolecules. 48:43-57
25. Rizzuto M, Marinetti L, Caretti D, Mugica A, Zubitur M, Müller AJ (2017) Can poly (ε-caprolactone) crystals nucleate glassy polylactide?. CrystEngComm. 19:3178
26. Di Lorenzo ML, Androsch R (2018) Influence of α′-/α-crystal polymorphism on properties of poly(l-lactic acid). Polym. Int. 0:1-15
27. Yokohara T, Yamaguchi M (2008) Structure and properties for biomass-based polyester blends of PLA and PBS. Eur. Polym. J. 44, 677-685
28. Shibata M, Inoue Y, Miyoshi M (2006) Mechanical properties, morphology, and crystallization behavior of blends of poly(L-lactide) with poly(butylene succinate-co-L-lactate) and poly(butylene succinate). Polymer. 47:3557-3564
29. Wu D, Yuan L, Laredo E, Zhang M, Zhou W (202) Interfacial Properties, Viscoelasticity, and Thermal Behaviors of Poly(butylene succinate)/Polylactide Blend. Ind. Eng.Chem. Res. 51:2290-2298
30. Dell'Erba R, Maglio G, Malinconico M, Migliozzi A (2001) Immiscible polymer blends of semicrystalline biocompatible components: thermal properties and phase morphology analysis of PLLA/PCL blends. Polymer. 42:7831-7840
31. Ostafinska A, Fortelny I, Nevoralova M, Hodan J, Kredatusova J, Slouf M (2015) Synergistic effects in mechanical properties of PLA/PCL blends with optimized composition, processing, and morphology. RSC Adv. 5, 98971-98982
32. Rizzuto M, Mugica A, Zubitur M, Caretti D, Müller AJ (2016) Plasticization and anti-plasticization effects caused by poly(L-lactide-ran-caprolactone) addition to double crystalline poly(L-lactide)/poly(ε- caprolactone) blends. CrystEngComm. 18:2014
33. Cordova ME, Lorenzo AT, Müller AJ, Gani L, Tence-Girault S, Leibler L (2011) The Influence of Blend Morphology (Co-Continuous or Sub-Micrometer Droplets Dispersions) on the Nucleation and Crystallization Kinetics of Double Crystalline Polyethylene/Polyamide Blends Prepared by Reactive Extrusion. Macromol. Chem. Phys. 212:1335-1350
34. Müller AJ, Avila M, Saenz G, Salazar J (2014) Crystallization of PLA-based Materials. In Jiménez A, Peltzer M, Ruseckaite R (eds) Poly(lactic acid) Science and Technology:

Processing, Properties, Additives and Applications. The Royal Society of Chemistry, Cambridge, UK, p 66-98

35. Di Lorenzo MR, Androsch R (2015) Crystallization of Poly(lactic acid). In: Fakirov S (ed) Biodegradable Polyesters. Wiley-VCH Verlag GmbH & Co. KGaA, Weinheim, Germany, p 109-130
36. Müller AJ, Arnal ML, Lorenzo AT (2013) Crystallization in Nano-Confined Polymeric Systems. In: Piorkowska E, Rutledge GC (eds) Handbook of polymer crystallization. John Wiley and Sons, Hoboken, New Jersey, 347-372
37. Sangroniz L, Barbieri F, Cavallo D, Santamaría A, Alamo RG, Müller AJ (2018) Rheology of self-nucleated poly(ε-caprolactone) melts. Eur. Polym. J. 99:495-503
38. Sangroniz L, Alamo RG, Cavallo D, Santamaría A, Müller AJ, Alegría A (2018) Differences between Isotropic and Self-Nucleated PCL Melts Detected by Dielectric Experiments. Macromolecules. 51:3663-3671
39. Müller AJ, Albuerne J, Esteves LM, Marquez L, Raquez JM, Degée Ph, Dubois Ph, Collins S, Hamley IW (2004) Confinement Effects on the Crystallization Kinetics and Self-Nucleation of Double Crystalline Poly(p-dioxanone)-b-poly(ϵ-caprolactone) Diblock Copolymers. Macromol. Symp. 215:369-382
40. Colonna S, Pérez-Camargo RA, Chen H, Liu G, Wang D, Müller AJ, Saracco G, Fina A (2017) Supernucleation and orientation of poly(butylene terephthalate) crystals in nanocomposites containing highly reduced Graphene Oxide. Macromolecules. 50:9380-9393
41. Pérez-Camargo RA, Fernández-d'Arlas B, Cavallo D, Debuissy T, Pollet E, Avérous L, Müller AJ (2017) Tailoring the Structure, Morphology, and Crystallization of Isodimorphic Poly(butylene succinate-ran-butylene adipate) Random Copolymers by Changing Composition and Thermal History. Macromolecules. 50:597-608
42. Righetti MC, Di Lorenzo ML, Tombari E, Angiuli M (2008) The low-temperature endotherm in poly(ethylene terephthalate): partial melting and rigid amorphous fraction mobilization. J. Phys. Chem. B. 112: 4233-4241
43. Righetti M C, Di Lorenzo ML (2016) Rigid amorphous fraction and multiple melting behavior in poly(butylene terephthalate) and isotactic polystyrene. J. Therm. Anal. Calorim. 126:521-530
44. Martin J, Stingelin N, Cangialosi D (2018) Direct calorimetric observation of the rigid amorphous fraction in a semiconducting polymer. J. Phys. Chem. Lett. 9: 990-995

45. Müller AJ, Balsamo V, Arnal ML, Jakob T, Schmalz H, Abetz V (2002) Homogeneous Nucleation and Fractionated Crystallization in Block Copolymers. Macromolecules. 35:3048-3058
46. Müller AJ, Balsamo V, Arnal ML (2005) Nucleation and Crystallization in Diblock and Triblock Copolymers. In: Abetz V (ed) Block Copolymers II. Springer Berlin Heidelberg, Berlin, p 1-63